◇論　文◇

Measuring Piping Erosion Rate in Bentonite Using Spectrophotometry and X-ray Computed Tomography

Ｘ線ＣＴと吸光光度法を用いたベントナイトの水みちによる流出速度の測定

OSAWA, Norihisa*;　ISHII, Tomoko*,**;
ISHII, Kenji***;　NIIBORI, Yuichi**

大　澤　紀　久*，　石　井　智　子*,**，
石　井　健　嗣***，　新　堀　雄　一**

ABSTRACT

In the geological disposal of high-level radioactive waste (HLW), a clay material called a buffer, usually made mainly of bentonite, is placed around the waste. The buffer is expected to serve several important functions, including limiting radionuclide migration, maintaining mechanical stability, and providing hydraulic control. However, in the environments with abundant groundwater, like Japan, bentonite may be eroded and transported by water flow. In particular, piping erosion can occur at the interface between the bentonite and the disposal pit wall, where water forms channels along the bentonite surface and carries the material away. This phenomenon is a significant concern because it may degrade the performance of the buffer.

In this study, we focused on measuring piping erosion in bentonite using X-ray computed tomography (CT) and spectrophotometry. X-ray CT was used to visualize the internal structure of the bentonite, as well as the piping channels formed along the bentonite surface, while spectrophotometry was used to measure the amount of bentonite in the outflow water.

The results showed that an index representing how easily bentonite is eroded (the apparent erosion rate constant) remained almost constant even when the water flow rate changed. This suggests that the amount of bentonite erosion caused by piping can be estimated using the index. Furthermore, this study demonstrated that X-ray CT would be a highly effective non-destructive tool for understanding bentonite behavior in buffer materials and providing time-dependent data.

Keywords ***:*** *X-ray CT, Bentonite, Buffer, Piping, Apparent erosion rate constant, Non-destructive tool*

＊株式会社太平洋コンサルタント　中央技術センター　電力・原子力技術部
Radioactive Waste Disposal Technology Department, Central Technology Center, Taiheiyo Consultant Co., Ltd.
＊＊東北大学
Tohoku University
＊＊＊鹿島建設株式会社
KAJIMA CORPORATION

要　旨

高レベル放射性廃棄物を地下に処分する際には、廃棄物の周りに「緩衝材」と呼ばれる粘土（ベントナイト）の層が設置され，核種の移行を抑制するなどの重要な役割を果たすことが期待されている．しかし，日本のように地下水が多い環境では，この粘土が水の流れによって削られ，流出する可能性がある．本研究では，X線CTと分光光度法を用いて，粘土が削られる際に発生する水みちの形状と流出量を詳しく測定した．その結果，水の流量が変わっても「見かけの流出速度定数(削られやすさを示す値)」はほぼ一定であることが分かった．この値を使えば，粘土の流出量を予測し，緩衝材の機能に及ぼす影響を評価できる可能性がある．また，X線CTが粘土の内部変化を非破壊で測定できる有効なツールであることも示された．

キーワード：X線CT，ベントナイト，緩衝材，水みち，見かけの流出速度定数，非破壊測定

1. INTRODUCTION

Geological disposal of high-level radioactive waste (HLW) relies on engineered barriers that include bentonite-based buffer materials, which are designed to limit groundwater flow and radionuclide migration. However, groundwater inflow can cause erosion of these materials through several mechanisms before they are fully saturated. Piping erosion is one of such processes in which flowing water forms a preferential pathway in partially saturated bentonite, leading to material loss. Other erosion mechanisms, including diffusion-driven erosion and colloid-facilitated transport, have also been reported; however, piping erosion is particularly critical during the early re-saturation phase of a disposal system when water inflow rates can be relatively high.

Research on piping erosion has been carried out internationally. For geological disposal of HLW in Japan, buffer materials consisting of bentonite and silica sand are considered for use in the engineered barriers, and research for its practical applications is ongoing by the Nuclear Waste Management Organization of Japan (NUMO) [1). One primary concern is the erosion of bentonite caused by groundwater flow. In Sweden and Finland, piping erosion has been investigated by the Swedish Nuclear Fuel and Waste Management Company (SKB) and Posiva, with groundwater inflow limits proposed to minimize the loss in buffer density during re-saturation [2), 3), 4)]. Several research institutes, such as the Centre for Energy, Environmental and Technological Research (CIEMAT) of Spain, have conducted bentonite diffusion experiments in sub-millimeter cracks as part of long-term erosion studies. These investigations also examined the roles of accessory minerals and soluble salts in detail [5)]. Recent studies have included water injection tests using Ca-type bentonite, with X-ray computed tomography (CT) being used to visualize the piping process. The experiments have shown that groundwater inflow can induce piping erosion and cracking [6)]. Furthermore, bentonite erosion has also been evaluated through analytical studies [7)].

Systematic investigations of bentonite erosion caused by piping began around 2000 in Japan. These studies have focused on the re-saturation period, which is the time from buffer emplacement in a vertical disposal pit to full recovery of the groundwater level, and used Kunigel V1 (Kunimine Industries Co., Ltd.) as a representative buffer material [8), 9)].

In Japan, groundwater inflow from the host rock remains abundant until the underground disposal repository is closed, which raised serious concern for the erosion-induced loss of bentonite from the buffer material that occurs shortly after its emplacement in the disposal pit. Considering the groundwater inflow conditions in Japan, tests were conducted in small cells under various conditions to understand the bentonite erosion phenomenon caused by piping [9)]. These tests were conducted with the water injection rate kept constant throughout each test. A correlation was found between the accumulated injected mass of water, M_w (g), and the accumulated dry mass of eroded montmorillonite, m_s (g), expressed as $m_s = 0.08M_w^{0.85}$. Subsequent scaled-up tests were conducted to understand bentonite erosion behavior and cumulative erosion volumes [10]. Additionally, erosion tests were conducted using real groundwater at the Horonobe Underground Research Laboratory in Japan [11].

As noted above, the quantitative evaluation of bentonite erosion has been based on the relationship between the cumulative amounts of injected water and the cumulative amounts of bentonite erosion. The NUMO also utilized the relationship for that purpose [1]. However, previous studies have relied on empirical relationships between cumulative injected water and cumulative mass loss and have not provided a generalized framework to predict erosion behavior. Therefore, this study aims to generalize the evaluation by directly quantifying the apparent erosion rate constant (i.e., specific erosion rate) of bentonite. Under constant flow conditions, piping tend to remain open. Meanwhile, under constant water pressure conditions, piping may gradually become blocked due to the expansion of bentonite [e.g., 12]. However, since the duration of blockage depends on the water pressure conditions, a constant flow rate was applied in the water injection tests conducted in this study as a conservative condition.

To achieve the purpose of the study, we combined in-situ X-ray CT, which allows for non-destructive visualization of the internal structure and evolution of piping, with spectrophotometric measurements of effluent bentonite concentrations. This combined approach enabled us to reconstruct the three-dimensional geometry of piping, calculate the surface area contributing to erosion, and develop a model that generalizes the erosion process beyond empirical formulas.

2. Materials & Methods

2.1 Materials

Two clay materials, Kunigel V1 and Kunipia F (Kunimine Industries Co., Ltd.), were used in this study. Kunigel V1 is a processed product of Na-bentonite quarried from the Tsukinuno Mine (Yamagata Prefecture, Japan). The physical properties of the clay material are known to vary between the lots. The Kunigel V1 used in this study had a montmorillonite content of 61%, along with accessory minerals such as quartz, clinoptilolite, feldspar, calcite, zeolite, and pyrite. The individual content rates of these accessory minerals were not measured in this study; instead, they were evaluated collectively as non-swelling particles in the piping erosion phenomenon. Kunipia F is a product obtained by removing accessory minerals from Kunigel V1 and refining it to achieve a montmorillonite content of 98% or higher [13]. Kunipia F was used to understand the dynamic piping erosion behavior of montmorillonite without accessory minerals, while Kunigel V1 was used to simulate the actual materials in practical use in Japan. In this study, bentonite was used alone, without silica sand, to avoid complications in X-ray CT analysis and modeling, thereby focusing on the fundamental erosion mechanisms.

Deionized water was used for the tests to eliminate effects of dissolved ions and study the physical processes of expansion and piping under controlled conditions.

2.2 Water injection test

Information about the specimens is shown in **Table 1**. Two types of tests were conducted using the specimens: one using Kunipia F (Test ID: F) and the other using Kunigel V1 (Test ID: V). Test specimens were prepared by statically compacting the material using a single-action die setup (50 mm in diameter, 50 mm in height). Although multi-layer compaction could potentially reduce vertical density variations in the specimens, single-layer compaction was employed in this study to eliminate the influence of layer boundaries which could otherwise cause development of preferential piping. To evaluate the influence of the accessory minerals, the dry weight of montmorillonite per unit volume was adjusted to approximately 1.0 Mg/m^3. This value refers exclusively to the montmorillonite fraction within the specimen and is defined as the product of the total dry density of the specimen and the montmorillonite content of the material used in its preparation.

Table 1　Physical and chemical properties of bentonite specimens used in this study.

Test ID	Product name	CEC and exchangeable cations* (meq/100g)					Total dry density (Mg/m^3)	Dry weight of montmo-rillonite per unit volume (Mg/m^3)	Swelling property
		Na^+	K^+	Mg^{2+}	Ca^{2+}	CEC			Swelling pressure** (MPa)
F	Kunipia F	110	1	3	20	133	1.0	1.0	(unknown)
V	Kunigel V1	64	1	1	17	79	1.6	1.0	1.5

* Values for Kunipia F were taken from published data [18], whereas values for Kunigel V1 were obtained experimentally in the present study.
** Swelling pressure of V was calculated from published data [19].

A polycarbonate cylindrical cell (PCC), with an inner diameter of 60 mm and a height of 50 mm, was used for the tests, allowing X-rays to penetrate easily. The specimen was placed with a 5-mm outer gap between the inner wall of the PCC and the specimen. The 5-mm annular gap was intentionally left around the specimen to simulate the inevitable gap that forms during buffer emplacement and to reproduce localized water inflow that can trigger piping. Deionized water was introduced through a bottom inlet using a flow pump with low pulsation (Tacmina, Q-100-6T) and distributed via a porous plate placed at the base of the PCC in laboratory temperature (20℃). The top of the specimen was left exposed to the air outside the cell, with excess water allowed to drain away. Overviews of the water injection test (the schematic diagram of the experimental apparatus and the structure of the PCC) are provided in **Fig. 1**. The valves connected to the PCC were closed when the shape of piping was stabilized at each flow rate. X-ray CT measurements, as described in the next section, were performed after the piping had reached a quasi-steady state to capture its geometry without further changes during the scanning process. When the valves were closed, the effluent was collected simultaneously.

After the tests, the concentration of bentonite in the outlet fluid was determined by measuring the absorbance at a wavelength of 350 nm using a spectrophotometer (Shimadzu, UV-2600). Standard suspensions of each clay material (Kunipia F and Kunigel V1) were also prepared in advance to obtain calibration curves relating the bentonite concentration to the absorbance, as shown in **Fig. 2(A)**. Although the term “bentonite concentration” is used in this study, previous

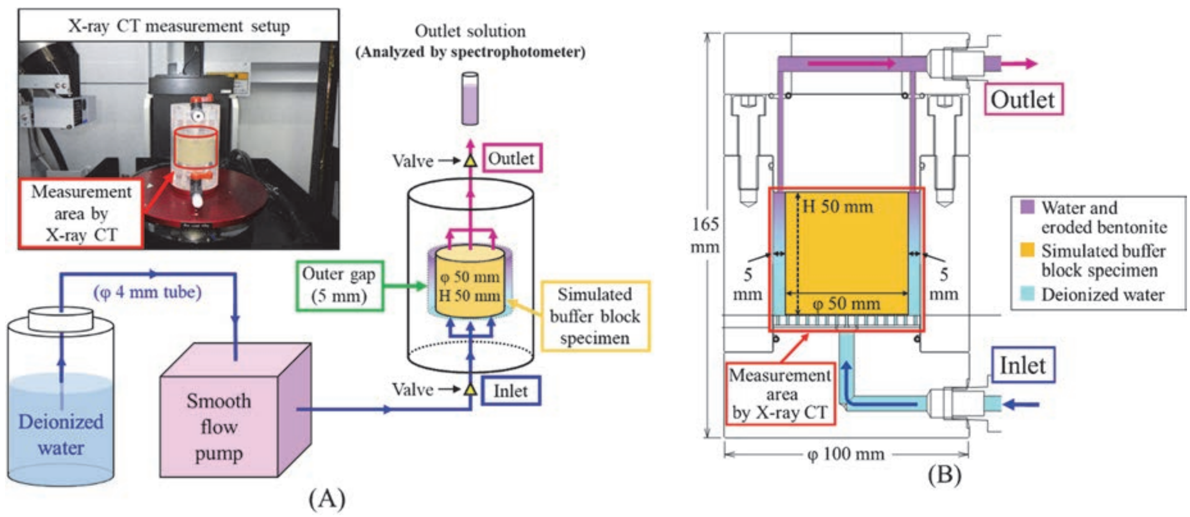

Fig. 1　Overviews of the water injection test: (A) Schematic diagram of the experimental apparatus, and (B) Structure of the PCC.

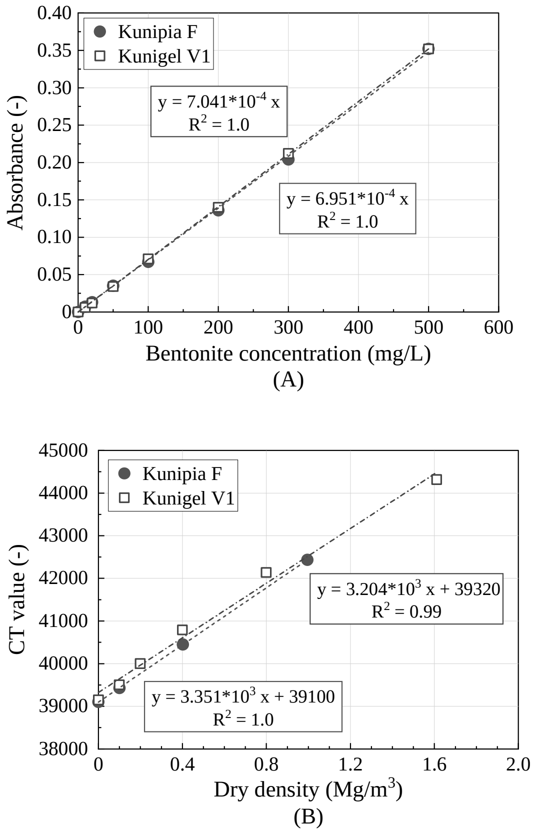

Fig. 2 Calibration curves indicating the relationship:
(A) bentonite concentration and absorbance,
(B) dry density and CT value.

studies (e.g., 10) have shown that the transported particles consist almost entirely of montmorillonite. In contrast, accessory minerals remain in the specimen and are not detected in the outlet fluid. Before analysis, a dispersant (Kanto Chemical, sodium hexametaphosphate) was added to these suspensions and outlet fluid, resulting in a total amount of 1% by weight in the liquid to be analyzed.

2.3 X-ray computed tomography measurement method

The inspeXio SMX 225CTS (Shimadzu Corporation), which offers high spatial resolution and excellent contrast, was used for X-ray CT measurements. Its performance enabled detailed imaging of piping geometry and detection of regions with densities lower than the solid particle density of bentonite (< 2.7 g/cm^3), which were essential for this study.

The X-ray CT measurements were performed under the conditions summarized in **Table 2**, with each scan taking approximately 5 minutes. To prevent blockage of piping due to bentonite swelling, water injection was temporarily suspended for a maximum of 10 minutes.

Several standard specimens using Kunipia F or Kunigel V1 were also prepared to obtain a calibration curve between the dry density and the X-ray CT measurement results in advance. These standard specimens were prepared by adding deionized water in increments to the clay materials in the PCC to achieve a specific density and fully saturate them with water. Subsequently, X-ray CT measurements were performed under the same conditions. As shown in **Fig. 2(B)**, the results indicate a strong correlation between the dry density and the X-ray CT measurement results. Furthermore, the threshold CT values corresponding to zero dry density for each clay material could be defined from these results (39100 CT units for Kunipia F and 39320 CT units for Kunigel V1).

After the X-ray CT measurements, dry density within the PCC was calculated from the calibration curve. Because simple thresholding was considered insufficient for extracting the piping due to noise and heterogeneity problems, a semi-manual procedure was employed. For consistency among the specimens, a fixed horizontal plane was extracted through the center of each specimen, and arc endpoints at that height

Table 2 Settings for X-ray CT measurements.

Settings	Values
X-ray tube voltage (kV)	200
X-ray tube current (μA)	70
Source to Detector Distance (SDD, mm)	800
Source to Rotation center Distance (SRD, mm)	160
X-ray filtering	None
Number of angles (/360°)	600
Total scan time (s)	300
Voxel size (mm/voxel)	0.039
XY cross-sectional image size (pixel)	2048x2048
Number of XY cross-sectional images	1580
3D image size (diameter, height, mm)	78.9, 61.6

were identified from automatically taken photos during each test. The corresponding CT image was then refined to delineate the boundary of the piping. Furthermore, in cases where threshold processing could not be performed in the depth direction, the cross-sectional area was calculated based on estimates using the endpoints obtained by the aforementioned method.

3. Results & Discussion

3.1 Water injection test

In this section, the test results are labeled using identifiers such as “F-1” to “F-7” and “V-1” to “V-7”, where “F” indicates specimens made from Kunipia F, and “V” indicates specimens made from Kunigel V1. The numbers represent individual test runs. The effluent bentonite concentration, c_{out} (kg/m^3), determined by the spectrophotometer is shown in **Table 3**, together with the water injection time until the stabilization of the shape of piping, p (min), the flow rate of water, Q (L/min), and the Reynolds numbers for the F and V tests. The calculated Reynolds numbers (**Table 3**) were all less than 10, indicating that laminar flow conditions prevailed throughout the tests.

The results showed gradual expansion of piping with the increase of the water flow rate. The position of piping in the F tests remained unchanged, whereas the shape and position of piping in the tests using Kunigel V1 changed because a different specimen was used from V-6 onwards. The reason for using different specimens was that the test plan had been extended beyond the initially planned flow rates, and a new specimen was prepared for the additional tests. The effluent concentration of bentonite in the F tests decreased from 2.052 kg/m^3 in F-1 to 0.136 kg/m^3 in F-7 with the increasing flow rates. The higher effluent concentration of bentonite in F-3 compared to F-2 was due to the swelling of bentonite during the CT measurements which caused temporary narrowing of the piping in part. When water injection was resumed at the start of F-3, a breakthrough may have occurred at the narrowed part, leading to a higher concentration of bentonite in the effluent. Similarly, in the tests using Kunigel V1, the effluent concentration of bentonite decreased from 5.150 kg/m^3 in V-1 to 0.365 kg/m^3 in V-7, with the increasing flow rates.

3.2 Modeling of bentonite erosion

To quantitatively characterize bentonite erosion caused by piping formation, a simplified model was developed using a single tortuous pipe with the following geometric parameters: length, l_p (m), horizontal cross-sectional area, s (m^2), and arc length excluding the PCC surface, l_{arc} (m). As illustrated in **Fig. 3**, three-dimensional (3D) and horizontal cross-sectional images obtained through X-ray CT enable the determination of the actual values of l_p, l_{arc}, and s. In this study, the values of l_{arc} and s along the piping were obtained from a single representative horizontal cross-section at a fixed position on the Z axis for all specimens, as shown in **Fig. 3**. Although piping geometry exhibited some variation within a specimen, measurements from this central horizontal slice were adopted as representative values for each test condition. The modeling approach utilized experimental data for the flow rate Q (m^3/s) and the concentration of eroded bentonite, c (kg/m^3), as determined by spectrophotometric analysis, under each test

Table 3　Injection conditions and effluent bentonite concentrations.

Test No.	Injection condition		Tests F		Tests V	
	Q (L/min)	Reynolds Number	p (min)	C_{out} (kg/m^3)	p (min)	C_{out} (kg/m^3)
1	1.0x10^{-4}	1.9x10^{-2}	2.4x10^3	2.052	5.8x10^4	5.150
2	5.0x10^{-4}	9.7x10^{-2}	6.0x10^1	1.312	6.0x10^1	3.984
3	1.0x10^{-3}	1.9x10^{-1}	6.0x10^1	1.412	6.0x10^1	2.394
4	2.0x10^{-3}	3.9x10^{-1}	6.0x10^1	0.591	3.0x10^1	1.508
5	5.0x10^{-3}	9.7x10^{-1}	6.0x10^1	0.347	3.0x10^1	1.041
6	1.0x10^{-2}	1.9x10^0	6.0x10^1	0.248	6.0x10^1	0.626
7	5.0x10^{-2}	9.7x10^0	6.0x10^1	0.136	1.2x10^2	0.365

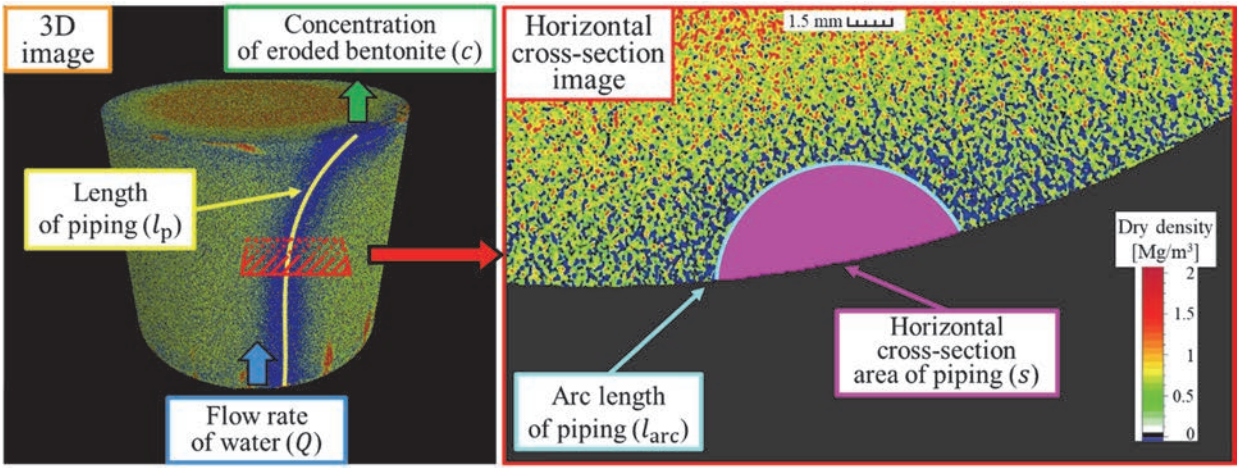

Fig. 3 Determination of geometric parameters (l_p, l_{arc}, and s) from 3D and horizontal cross-sectional images obtained by X-ray CT.

condition. The detailed modeling process is described below.

Following the formation of piping, both the arc length l_{arc} and the cross-sectional area s stabilized rapidly. The specific arc length, a (= l_{arc}/s, 1/m), remained approximately constant throughout the experimental period under the same conditions. The stability of piping was determined through both photographs and X-ray CT images. Therefore, the present study assumes that bentonite erosion from the piping wall (excluding the PCC surface) occurs at a constant rate, and that eroded material is transported with the fluid to the outlet through the advective processes.

Under the assumption of an incompressible fluid flow within the pipes, the flow velocity, $u = Q/s$, remains constant. Furthermore, assuming that bentonite erosion follows zero-order reaction kinetics, the mass balance equation for bentonite concentration, c, within the piping can be expressed as

$$\frac{\partial c}{\partial t} = -u\frac{\partial c}{\partial x} + ak \ , \quad (1)$$

where k (kg/(m^2·s)) represents the apparent erosion rate constant (i.e., specific erosion rate) which is defined as the mass of bentonite eroded per unit surface area per unit time. This equation is derived from the so-called "advection-dispersion equation with zero-order reaction" which is commonly used to model the mass balance in pipes by disregarding the dispersion term when the advection term is dominant (e.g., 14). It is further assumed that the concentration distribution in the x-direction immediately reaches a steady state, because the reaction (erosion) time is significantly larger than the mean residence time of the fluid in the piping, $t^* = l_p/u$ (e.g., 15). Under these conditions, the pseudo-steady-state approximation for c in Equation (1) yields

$$u\frac{dc}{dx} = ak \ . \quad (2)$$

Equation (2) can be separated into variables and integrated by applying the boundary conditions $c = c_{in}$ at $x = 0$ (influent concentration of bentonite) and $c = c_{out}$ at $x = l_p$ (effluent concentration), which yields

$$\int_{c_{in}}^{c_{out}} dc = \int_0^{l_p} \frac{ak}{u} dx \ , \quad (3)$$

which simplifies to

$$c_{out} - c_{in} = \frac{ak}{u} l_p \ . \quad (4)$$

Since cin can be set to zero and a expressed as larc/s, the apparent erosion rate constant k can be calculated as

$$k = \frac{Q \cdot c_{out}}{l_{arc} \cdot l_p} \ , \quad (5)$$

where Q·cout represents the erosion rate (mass per unit time). The apparent erosion rate constant k was evaluated by substituting the experimentally determined values of Q, cout, larc, and lp from each test condition into Equation (5).

3.3 Apparent erosion rate constant of bentonite

The piping sizes and the calculated values of k for the F and V tests are presented in **Table 4** and **5**, respectively. **Fig. 4** shows the examples of images from both tests, including 3D views, extracted horizontal cross-sectional CT slices, and external photographs. (Please contact us if you want to check the supplementary materials for all test photographs and X-ray CT images.)

In this study, k was calculated using the dimensions of the stabilized piping at the end of each test, because the purpose was to relate k to the stable geometry that controls the flow conditions in the subsequent test. The first data point (5mm gap → piping) was treated separately due to its different initial condition.

As the bentonite was washed away from the surface of the piping, the density around the piping was found to decrease in both the F and V tests, with its heterogeneity increasing. Furthermore, only slight changes were observed in the actual length of the piping, even as the water flow rate was increased. The tortuosity of the piping, defined as the ratio of its actual length to the straight-line distance between its endpoints, remained nearly constant (close to 1) in both the F and V tests.

Moreover, as shown in **Fig. 5(A)**, the erosion rate of bentonite ($Q \cdot c_{out}$) was proportional to the actual arc length of the piping (l_{arc}). In other words, the quotient $Q \cdot c_{out}$ / l_{arc} remained nearly constant throughout the experiments. Additionally, as

Table 4 Size of piping and apparent erosion rate constant in test F.

Test No.	Actual arc length of piping (l_{arc}, m)	Length of piping (l_p, m)		Apparent erosion rate constant (k, kg/(m^2·s))	
		Straight-line	Actual	Individual	Average* (excluding F-1)
F-1	0.420×10^{-3}	5.085×10^{-2}	5.257×10^{-2}	1.55×10^{-4}	$2.40 \times 10^{-4} \pm 3.78 \times 10^{-5}$
F-2	0.780×10^{-3}	5.093×10^{-2}	5.187×10^{-2}	2.70×10^{-4}	
F-3	1.323×10^{-3}	5.043×10^{-2}	5.833×10^{-2}	3.05×10^{-4}	
F-4	1.671×10^{-3}	5.192×10^{-2}	5.780×10^{-2}	2.04×10^{-4}	
F-5	2.646×10^{-3}	5.144×10^{-2}	5.581×10^{-2}	1.96×10^{-4}	
F-6	3.299×10^{-3}	5.172×10^{-2}	5.542×10^{-2}	2.26×10^{-4}	
F-7	8.753×10^{-3}	5.189×10^{-2}	5.386×10^{-2}	2.41×10^{-4}	

* The averages and standard deviations were calculated excluding the first data points (F-1).

Table 5 Size of piping and apparent erosion rate constant in test V

Test No.	Actual arc length of piping (l_{arc}, m)	Length of piping (l_p, m)		Apparent erosion rate constant (k, kg/(m^2·s))	
		Straight-line	Actual	Individual	Average* (excluding V-1)
V-1	1.201×10^{-3}	5.206×10^{-2}	5.513×10^{-2}	1.30×10^{-4}	$3.80 \times 10^{-4} \pm 5.72 \times 10^{-5}$
V-2	1.480×10^{-3}	5.174×10^{-2}	5.387×10^{-2}	4.16×10^{-4}	
V-3	2.040×10^{-3}	5.268×10^{-2}	5.421×10^{-2}	3.61×10^{-4}	
V-4	2.251×10^{-3}	5.145×10^{-2}	5.237×10^{-2}	4.26×10^{-4}	
V-5	3.845×10^{-3}	5.112×10^{-2}	5.142×10^{-2}	4.39×10^{-4}	
V-6	7.652×10^{-3}	5.021×10^{-2}	5.051×10^{-2}	2.70×10^{-4}	
V-7	1.672×10^{-2}	4.930×10^{-2}	4.958×10^{-2}	3.67×10^{-4}	

* The averages and standard deviations were calculated excluding the first data points (V-1).

shown in **Fig. 5(B)**, the apparent erosion rate constants (k) for Kunipia F and Kunigel V1 were nearly constant regardless of the water flow rate (Q). These findings support the consistency of Equation (5), considering that the piping length (l_p) was essentially constant in all cases.

Furthermore, as shown in **Fig. 5(C)**, a strong correlation was found between the water flow rate and the actual arc length of the piping. The actual arc length of piping formed in the Kunigel V1 specimens was longer than that in the Kunipia F specimens. As previously described, the effluent concentration of bentonite (c_{out}) can be estimated by using the apparent erosion rate constant (k), the actual arc length of the piping (l_{arc}), the total length of the piping (l_p), and the flow rate (Q). This is possible because the apparent erosion rate constant remains unchanged under the given conditions.

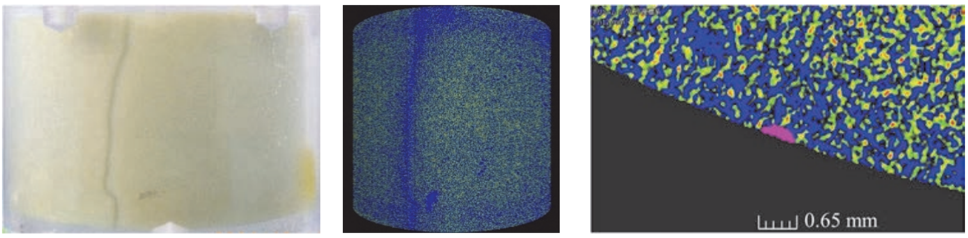

(A) F-2 (Q = 5.0x10^{-4} L/min)

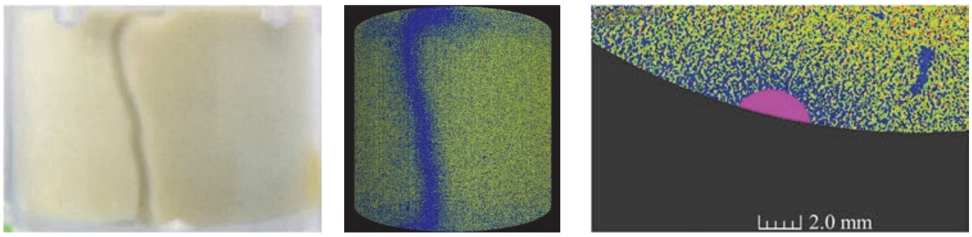

(B) F-5 (Q = 5.0x10^{-3} L/min)

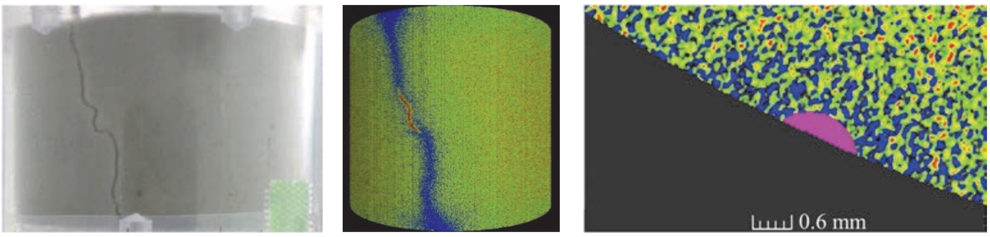

(C) V-2 (Q = 5.0x10^{-4} L/min)

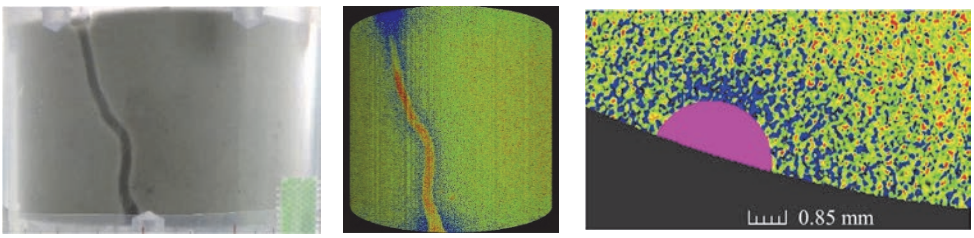

(D) V-5 (Q = 5.0x10^{-3} L/min)

Fig. 4 Examples of exterior photographs (left column), 3D images obtained by X-ray CT (middle column), and horizontal cross-sectional images obtained by X-ray CT (right column).

3.4 Effect of the montmorillonite content ratio

The montmorillonite content was different between Kunipia F and Kunigel V1. However, the apparent erosion rate constants were nearly identical between the F and V tests. Although the average value for the V test specimens was about 1.5 times that for the F test specimens, the variation within each group was significant, and the difference in the average values was interpreted as being within the experimental scatter. The similarity between the two groups can be attributed to the fact that their effective clay densities were adjusted to comparable levels (0.96-0.99 Mg/m^3) which resulted in similar swelling pressures (up to 1.2 MPa). These findings suggest that effective clay density, which governs swelling pressure and resistance to shear stress, plays a key role in controlling erosion behavior. Nonetheless, the apparent erosion rate constant of bentonite for the V test specimens was slightly higher than that for the F test specimens. This slight difference may be related to the higher content of accessory minerals contained in Kunigel V1. The presence of more accessory minerals likely led to formation of a more heterogeneous microstructure around piping, in the sense of spatial variation in bentonite density and water accessibility. Where accessory minerals accumulated on the piping surfaces (as shown in **Fig. 4(D)**), the bentonite–water contact was partially blocked. Although low-density regions were not directly observed, it was inferred that localized low densities might have existed in adjacent areas where the buildup of accessory minerals reduced the space available for montmorillonite. These weaker areas appear to have been preferentially eroded, resulting in a slightly higher overall erosion rate in the V test specimens. Nevertheless, the detailed mechanism remains uncertain and should be investigated further.

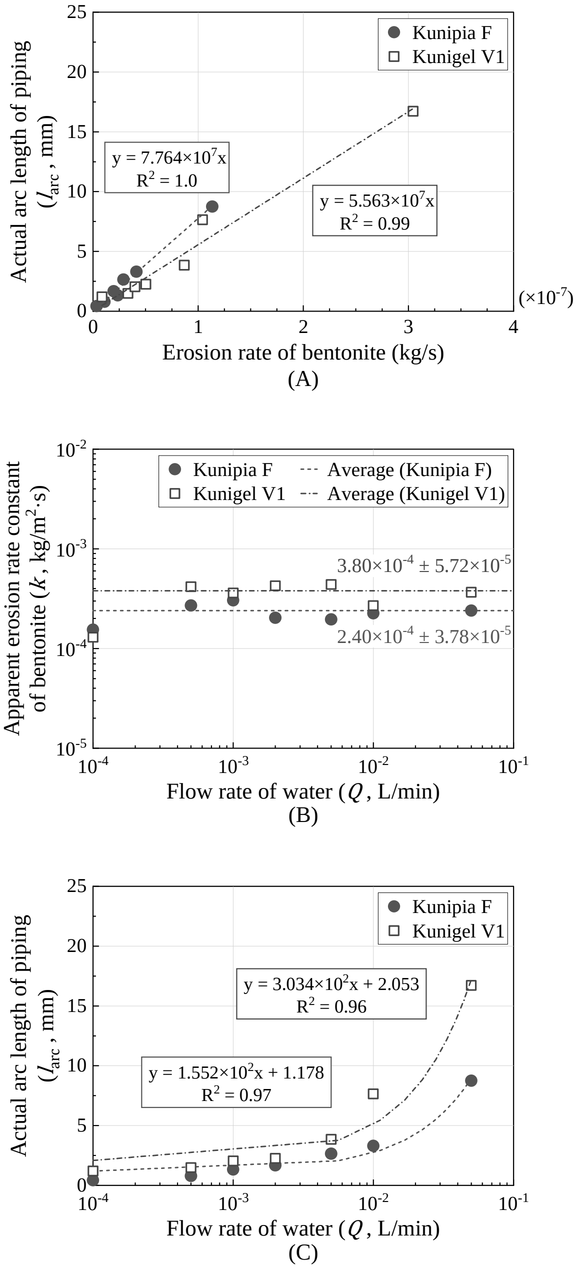

Fig.5 Correlation of each parameter.

3.5 Scenario-based estimation of long-term bentonite erosion

To estimate the potential impact of bentonite erosion under repository conditions, a scenario calculation was performed using the obtained apparent erosion rate constant, k, and assuming a groundwater flow from the bottom to the top of a vertical disposal hole. A conservative groundwater flow rate of 0.1 L/min was assumed, based on the upper bound considered by the SKB [16], which is also referenced in the NUMO's design basis [1]. This flow rate exceeds those tested in the present study and therefore represents an extrapolation.

Using $k \approx 2.5 \times 10^{-4}$ kg/(m^2·s), an arc length of 32.4 mm, and an effluent concentration of 27.76 kg/m^3, the bentonite loss was estimated to be approximately 4 x 10^{-3} Mg/day. Given the NUMO's allowable erosion limit of 0.45 Mg, this corresponds to 112 days of continuous erosion under the assumed conditions.

According to the NUMO's comprehensive safety assessment report—appendix [17], the evaluation period for buffer erosion is defined as the time before tunnel backfilling and generally ranges from 284 to 459 days, depending on the geological environment and repository concept. Compared to that period, the estimated 112 days is significantly shorter, indicating a relatively high erosion rate under conservative assumptions.

However, the current scenario does not fully reflect in situ conditions. The assumption of a continuous flow rate of 0.1 L/min and a constantly open and stable piping likely overestimates erosion. While stabilized piping was observed in laboratory tests, whether this occurs under repository conditions and persists over time remains uncertain. If bentonite swelling leads to self-sealing, erosion would be significantly reduced; otherwise, erosion may continue at a reduced rate.

Additionally, the present study is based on small-scale laboratory tests using the bentonite blocks without the addition of silica sand. In contrast, actual repositories typically use bentonite-silica sand mixtures, and groundwater chemistry (e.g., salinity, divalent cations) can influence erosion behavior. Therefore, while the simplified model provides a proper estimate, its applicability to real-scale repository conditions must be considered with caution.

4. Conclusions

This study quantitatively evaluated bentonite erosion caused by piping using a combination of controlled flow-through tests, X-ray computed tomography (CT), and spectrophotometric analysis of effluent suspensions. CT images provided three-dimensional reconstructions of piping, and integrating the geometric data with effluent concentrations enabled a mass-balance description of the erosion process.

In the tests, Kunipia F, with a 98% montmorillonite content, and Kunigel V1, a bentonite containing 61% montmorillonite and accessory minerals, were used as materials. Within the flow rate range of these tests, the apparent erosion rate constant k remained nearly constant, concentrated around 2-3 $\times 10^{-4}$ kg/(m^2·s), with only a slight difference between the two materials. This may be because their dry weights of montmorillonite per unit volume were nearly the same. The erosion rate, expressed as the product of flow rate and effluent concentration, was found to increase with the increase of the piping arc length and be consistent with surface-controlled removal of bentonite along the piping wall. The slightly higher k for Kunigel V1 is plausibly related to accessory-mineral-induced heterogeneity around the piping. These results support the applicability of a simple geometry-based mass-balance model for predicting effluent concentrations when the piping geometry is known.

A conservative scenario calculation based on the measured k indicates that, under a constant groundwater inflow of 0.1 L/min, the allowable erosion could be reached in approximately 100 days. However, this estimate likely overstates in-situ losses because self-sealing effect would work under the actual repository conditions, and the present tests were conducted using small-scale bentonite blocks without silica sand admixture. Future work should extend the investigation to bentonite-silica sand mixtures, relevant groundwater chemistries, and pressure-controlled boundary conditions to better capture the development of piping.

In particular, the X-ray CT technique employed in this study has proved to be effective in non-destructive visualization of piping in three dimensions and quantitative analysis of its geometry. Applying this method to actual material compositions and groundwater conditions is expected to make a substantial contribution to developing more realistic long-term performance assessments with enhanced reliability.

REFERENCES

1) Nuclear Waste Management Organization of Japan. The NUMO Pre-siting SDM-based Safety Case (NUMO-TR-21-01). 2021.
2) Lennart Börgesson, Torbjörn Sandén. Piping and erosion in buffer and backfill materials: Current knowledge (SKB Rapport R-06-80). Svensk kärnbränslehantering AB. 2006.
3) Torbjörn Sandén, Lennart Börgesson. Deep repository-engineered barrier system: Piping and erosion in tunnel backfill: Laboratory tests to understand processes during early water uptake (SKB Rapport R-06-72). Svensk kärnbränslehantering AB. 2008.
4) Petri Sane, Teemu Laurila, Markus Olin et al. Current Status of Mechanical Erosion Studies of Bentonite Buffer (Posiva Report, POSIVA 2012-45). Posiva Oy. 2013.
5) Ursula Alonso, Tiziana Missana, Miguel García Gutiérrez et al. CIEMAT studies within POSKBAR Project: Bentonite expansion, sedimentation and erosion in artificial fractures (Technical Report SKB TR-19-08). Svensk kärnbränslehantering AB. 2019.
6) Minhyeong Lee, Chang-Ho Hong, Ji-Won Kim et al. Early and post-stage piping erosion in bentonite buffer materials exposed to groundwater inflow. Geomechanics for Energy and the Environment. 2024, 40, e100611.
7) Arnau Pont, Andrés Idiart. Numerical model for the quantification of buffer bentonite mass losses due to expansion, erosion and sedimentation (Posiva SKB Report 13). Svensk kärnbränslehantering AB. 2024.
8) Radioactive Waste Management Funding and Research Center. Heisei 23 nendo Chisō shobun gijutsu chōsa-tō jigyō: Kōreberu hōshasei haikibutsu shobun kanren: Shobun shisutemu kōgaku yōso gijutsu kōdo-ka kaihatsu Hōkokusho (Dai 2 bunsatsu) － Jinkō baria hinshitsu hyōka gijutsu no kaihatsu－ (2 / 2). 2012. (in Japanese). https://warp.ndl.go.jp/web/20200201212630/www.enecho.meti.go.jp/category/electricity_and_gas/nuclear/rw/library/2011/23-8-2-2.pdf, (accessed 2026-03-25)
9) K. Suzuki, H. Asano, R. Yahagi et al. Experimental investigations of piping phenomena in bentonite-based buffer materials for an HLW repository. Clay Minerals. 2013, 48(2), p.363-382.
10) Tomoko ISHII, Masahiro KAWAKUBO, Ichizo KOBAYASHI et al. Experimental approach for understanding the dynamic behaviors of bentonite buffer piping erosion. Mechanical Engineering Journal. 2020, 7(3), e19-00469.
11) Mayumi Jo, Makoto Ono, Masashi Nakayama et al. A study of methods to prevent piping and erosion in buffer materials intended for a vertical deposition hole at the Horonobe Underground Research Laboratory. Geological Society Special Publication; Multiple Roles of Clays in Radioactive Waste Confinement. 482(1), 2018, p.175-190.
12) Japan Atomic Energy Agency, Radioactive Waste Management Funding and Research Center. Reiwa 3 nendo Kōreberu hōshasei haikibutsu-tō no chisō shobun ni kansuru gijutsu kaihatsu jigyō: Nia-fīrudo shisutemu hyōka kakushō gijutsu kaihatsu Hōkokusho. 2022. (in Japanese) . https://www.enecho.meti.go.jp/category/electricity_and_gas/nuclear/rw/library/2021/3fy_nf.pdf, (accessed 2026-03-25)
13) KUNIMINE INDUSTRIES. “KUNIPIA-F: Safety Data Sheet”. 2025. (in Japanese).
14) Takenori Ozutsumi, Masayuki Kogure, Yuichi Niibori et al. Fundamental Study on Transport Model for Radionuclides under Unsaturated Condition around Near-Surface Underground. MRS Advances. 2020, 5(5-6), p.223-232.
15) Tsugumi Seki, Kazuki Furiya, Taiji Chida et al. Evaluation of the Changes in Effective Fracture Aperture with Deposition of Calcium Silicate Hydrate on Granite Surface Under Highly Alkaline Saline Conditions Using a Microflow Cell. ACS ES&T Water. 2024, 4(4), p.1864-1873.
16) Torbjörn Sandén, Lennart Börgesson. Early effects of water inflow into a deposition hole: Laboratory tests results (SKB Report R-10-70). Svensk kärnbränslehantering AB., 2010.

17) Nuclear Waste Management Organization of Japan. Appendix SR 4-56; Evaluation of piping erosion of buffer. The NUMO Pre-siting SDM-based Safety Case; Appendix (NUMO-TR-20-03). 2021. (in Japanese).
18) Yasutaka WATANABE, Shingo YOKOYAMA. Evaluation of Montmorillonite Content of Bentonite Considering Accuracy of Methylene Blue Adsorption Test. Journal of Japan Society of Civil Engineers, Ser. C (Geosphere Engineering). 2020, 76(1), p.26-39. (in Japanese).
19) Hirohito KIKUCHI, Kenji TANAI. Basic characteristic test of buffer / backfill material under Horonobe groundwater condition (Testing Document) (JNC TN8430 2004-005). Japan Nuclear Cycle Development Institute. 2005. (in Japanese).